Dynamics in multiple-well Bose-Einstein condensates

M. Nigro, P. Capuzzi, H. M. Cataldo, and D. M. Jezek
Universidad de Buenos Aires, Facultad de Ciencias Exactas y Naturales, Departamento de Física, Buenos Aires, Argentina and IFIBA, CONICET-UBA, Pabellón 1, Ciudad Universitaria, 1428 Buenos Aires, Argentina

(Received 13 October 2017; published 24 January 2018)

We study the dynamics of three-dimensional weakly linked Bose-Einstein condensates using a multimode model with an effective interaction parameter. The system is confined by a ring-shaped four-well trapping potential. By constructing a two-mode Hamiltonian in a reduced highly symmetric phase space, we examine the periodic orbits and calculate their time periods both in the self-trapping and Josephson regimes. The dynamics in the vicinity of the reduced phase space is investigated by means of a Floquet multiplier analysis, finding regions of different linear stability and analyzing their implications on the exact dynamics. The numerical exploration in an extended region of the phase space demonstrates that two-mode tools can also be useful for performing a partition of the space in different regimes. Comparisons with Gross-Pitaevskii simulations confirm these findings and emphasize the importance of properly determining the effective on-site interaction parameter governing the multimode dynamics.

DOI: 10.1103/PhysRevA.97.013626

I. INTRODUCTION

The experimental research on Bose-Einstein condensates trapped in ring-shaped optical lattices constitutes a promising area that is meant to open the possibility to study a rich emerging physics. Consequently, important efforts are being made towards the effective realization of such configurations [1–3]. For instance, a lattice of tunnel junctions on a ring would enable the creation of lattice models with periodic boundary conditions and with the resulting ability to support piercing magnetic fluxes and the associated topological phenomena [3]. In particular, it would provide an ideal environment for the study of the Kibble-Zurek mechanism, where the buildup of winding number in the phase transition from Mott insulator to superfluid driven by tunneling rate increase is expected to occur, except for very slow quench times [4]. On the other hand, quantum information applications of such configurations have begun to be devised, such as the experimentally feasible qubit system based on bosonic cold atoms trapped in ring-shaped optical lattices, proposed by Amico *et al.* [5]. A practical implementation of this system could lead to substantially lower decoherence rates, as the use of neutral atoms as flux carriers would minimize the well-known characteristic fluctuations in the magnetic fields of solid-state Josephson qubits.

Concerning theoretical studies on this issue, the dynamics on ring lattices with three [6] and four [7] wells have been previously investigated through multimode (MM) models that utilized *ad hoc* values for the hopping and on-site energy parameters. Substantial improvements were reported in Ref. [8], where such parameters were calculated *ab initio* by constructing a set of two-dimensional localized wave functions in terms of the stationary solutions of the Gross-Pitaevskii (GP) equation for a ring with an arbitrary number of wells. This can be regarded as a similar procedure to the two-mode (TM) model of a double-well condensate [9–16], where the order parameter is described as a superposition of wave functions localized in each well with time-dependent coefficients [9,10]. Such localized wave functions are straightforwardly obtained in terms of the stationary symmetric and antisymmetric states, which in turn determine the parameters involved in the TM equations of motion [9–12]. The corresponding dynamics exhibits Josephson and self-trapping regimes [9,10], which have been experimentally observed by Albiez *et al.* [13]. The self-trapping (ST) phenomenon, which is also present in extended optical lattices [17–19], is a nonlinear effect where the difference of populations between neighboring sites does not change sign during the whole time evolution. There is nowadays active research on the ST effect, which involves different types of systems, including mixtures of atomic species [14,20].

In recent works, it has been shown that the on-site interaction energy dependence on the population imbalance has to be taken into account for the TM model in order to accurately describe the exact dynamics in double-well systems [8,21,22]. Such an imbalance dependence gives rise to a reduced effective on-site interaction energy parameter when it is introduced into the equations of motion of the model. In the Thomas-Fermi approximation, it has been shown that such a parameter is reduced by a factor of 7/10, 3/4, or 5/6 depending on the dimensionality of the system. Later, it was proven that the effective on-site interaction energy parameter is also fundamental to describe the dynamics in a ring-shaped lattice, within the frame of MM models in two-dimensional condensates as well [8].

The phase space of a MM dynamics in a N_c-well system has $2N_c - 2$ dimensions. Hence, the analysis of such a dynamics for $N_c \geqslant 3$ does not pose a simple task to handle. The goal of this work is to show that useful results can still be obtained by using mathematical tools such as symmetry criteria and special techniques developed for nonlinear differential equations [23]. In particular, we will numerically treat a three-dimensional

four-site ring-shaped optical lattice. The construction of its multimode parameters will be based on previous works [8,24], where a method to obtain localized on-site Wannier-like (WL) functions in a ring-shaped optical lattice was developed. These states are obtained as a superposition of stationary states of the GP equation with different winding numbers. Here we will show how to optimally localize these WL states to finally obtain the effective on-site interaction energy parameter for furnishing an accurate model. On the other hand, by restricting the dynamics to a symmetric case, we will construct a two-mode-type Hamiltonian able to predict transitions to the ST regime. With such a Hamiltonian, we will calculate the orbit periods in both Josephson and ST regimes. Next, we will show that the location of the two-mode critical point of the Josephson to ST transition turns out to be quite useful to determine the domains of different regimes in an extended region compared to that of the symmetric case. These findings will be confirmed by local TM models involving only pairs of neighboring sites [18,19]. Finally, by calculating Floquet multipliers [23], we will analyze the dynamical stability in the surroundings of the TM solutions and we will show that in the more stable regions, a criteria for calculating characteristic times can be established.

This paper is organized as follows. In Sec. II, we describe the trapping potential and include the equations of motion of the MM model. Next, we explain the procedure for obtaining the localized states used to describe the dynamics and analyze the conditions to achieve maximally localized WL functions. To conclude this section, we summarize the method for calculating the effective on-site energy parameter and analyze the corresponding results of a few representative configurations. In Sec. III A, we numerically study the dynamics, showing that one can predict the ST and Josephson regimes using a reduced-space Hamiltonian that describes high-symmetry systems. This reduction allows us to extend previous analytic results of the period of the trajectories in the TM model to these systems. Next, in Sec. III B, we study the dynamics close to this highly symmetric situation by means of a Floquet analysis. Finally, in Sec. III C, we numerically obtain the MM dynamics for nonsymmetric configurations in the vicinity of the symmetric condition, establishing useful connections to the symmetric case results and comparing with several full GP solutions. To conclude, a summary of our work is presented in Sec. IV. The definitions of the parameters employed in the equations of motion are gathered in Appendix A, while in Appendix B we give some details of the Floquet analysis theory.

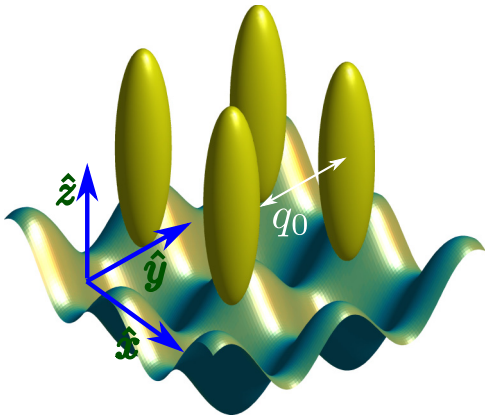

FIG. 1. Isosurfaces of the ground-state density and the trapping potential of the four-site system with $N = 10^4$ and $V_b/\hbar\omega_x = 25$ (in arbitrary units).

II. THE MULTIMODE MODEL

A. The trap

We consider a three-dimensional Bose-Einstein condensate of rubidium atoms confined by the external trap,

$$V_{\rm trap}(\mathbf{r}) = \tfrac{1}{2}\, m \left[\omega_x^2 x^2 + \omega_y^2 y^2 + \omega_z^2 z^2\right] + V_b[\cos^2(\pi x/q_0) + \cos^2(\pi y/q_0)], \quad (1)$$

where m is the atom mass. The harmonic frequencies are given by $\omega_x = \omega_y = 2\pi \times 70$ Hz and $\omega_z = 2\pi \times 90$ Hz, and the lattice parameter is $q_0 = 5.1\ \mu$m. The barrier height parameter V_b and the number of particles will take different values upon the calculation. For instance, in Fig. 1, we have plotted isosurfaces of the ground-state density and the trapping potential for $N = 10^4$ and $V_b/(\hbar\omega_x) = 25$. Hereafter, time and energy will be given in units of ω_x^{-1} and $\hbar\omega_x$, respectively.

B. Equations of motion

For completeness, in this section we will sketch the procedure for obtaining the equations of motions reported in Ref. [8]. The multimode order parameter for N_c sites is expressed in terms of N_c localized WL functions w_k as

$$\psi(\mathbf{r})_{\rm MM} = \sum_k b_k(t)\, w_k(r,\theta,z), \quad (2)$$

where $-[(N_c-1)/2] \leqslant k \leqslant [N_c/2]$. Inserting the above expression into the time-dependent GP equation, the equations of motion for the coefficients $b_k(t) = e^{i\phi_k}\,|b_k|$ are obtained, which can be cast into $2N_c$ real equations for the populations $n_k = |b_k|^2 = N_k/N$ and the phase differences $\varphi_k = \phi_k - \phi_{k-1}$ of each site as

$$\hbar\,\frac{dn_k}{dt} = -2J[\sqrt{n_k\, n_{k+1}}\,\sin\varphi_{k+1} - \sqrt{n_k\, n_{k-1}}\,\sin\varphi_k] - 2F[\sqrt{n_k\, n_{k+1}}(n_k + n_{k+1})\,\sin\varphi_{k+1} - \sqrt{n_k\, n_{k-1}}(n_k + n_{k-1})\,\sin\varphi_k], \quad (3)$$

$$\hbar\frac{d\varphi_k}{dt} = N(U_{k-1}n_{k-1} - U_k n_k) - J\left[\left(\sqrt{\frac{n_k}{n_{k-1}}} - \sqrt{\frac{n_{k-1}}{n_k}}\right)\cos\varphi_k + \sqrt{\frac{n_{k-2}}{n_{k-1}}}\cos\varphi_{k-1} - \sqrt{\frac{n_{k+1}}{n_k}}\cos\varphi_{k+1}\right]$$
$$- F\left[\left(n_k\sqrt{\frac{n_k}{n_{k-1}}} - n_{k-1}\sqrt{\frac{n_{k-1}}{n_k}}\right)\cos\varphi_k + \left(3\sqrt{n_{k-2}\,n_{k-1}} + n_{k-2}\sqrt{\frac{n_{k-2}}{n_{k-1}}}\right)\cos\varphi_{k-1}\right.$$
$$\left. - \left(3\sqrt{n_{k+1}\,n_k} + n_{k+1}\sqrt{\frac{n_{k+1}}{n_k}}\right)\cos\varphi_{k+1}\right], \tag{4}$$

where U_k is the on-site interaction energy in the k site. The bare MM model assumes a constant $U_k = U$ value. In contrast, in the effective MM model, its dependence on the imbalance is considered $U_k = U_k(\Delta N_k)$, which gives rise to a reduced effective parameter $U_{\rm eff}$ (see Sec. II D). The definitions of the bare interaction parameter U and the tunneling parameters J and F are given in Appendix A. As the populations and phase differences must fulfill $\sum_k n_k = 1$ and $\sum_k \varphi_k = 0$, respectively, only $2N_c - 2$ equations are independent. In Eq. (4), we have excluded the terms involving the overlap between the localized densities in each site, as this parameter turns out to be two orders of magnitude smaller than the rest of the tunneling parameters, J and F.

C. Localized states and multimode model parameters

In this section, we summarize the procedure to obtain the localized states [8,24] necessary to describe the dynamics. The choice of these states is not unique, as they inherit the freedom in the choice of the global phase of stationary states. In the field of atomic and molecular physics, the concept of localized molecular orbitals, or "Boys orbitals," in chemistry has been long applied, and after that in electronic calculations in periodic systems (see, e.g., the review of Ref. [25] and references therein) in order to optimize the basis set used. We will therefore analyze how the localization of the WL functions affects the determination of the model parameters, especially the on-site energy parameter U.

The stationary states $\psi_n(r,\theta,z)$ are obtained as the numerical solutions of the three-dimensional GP equation [26] with different winding numbers n [8,27]. Assuming large barrier heights [24], the winding numbers will be restricted to the values $-[(N_c-1)/2] \leqslant n \leqslant [N_c/2]$ [27]. We have shown in Ref. [24] that stationary states of different winding number are orthogonal and can be used to define localized, orthogonal, WL functions on each k site. These are given by

$$w_k(r,\theta,z) = \frac{1}{\sqrt{N_c}}\sum_n \psi_n(r,\theta,z)\, e^{-in\theta_k}, \tag{5}$$

where $\theta_k = 2\pi k/N_c$.

The ground state ($n = 0$) and the state with maximum winding number, i.e., $n = 2$ for the four-site system, have completely uniform phases in each well [27]. Both functions can be chosen to be real with $\psi_0 > 0$ and $\psi_2 > 0$ in the first quadrant ($0 < \theta < \pi/2$). This means that we have fixed their phases to zero in that quadrant. On the other hand, the winding numbers with $n = \pm 1$ correspond to vortexlike states, which have an associated velocity field that gives rise to a nonvanishing angular momentum [27]. Although their velocity fields are very small in each site, the phase is not absolutely uniform and, to perform the sum of Eq. (5), it is important to correctly choose the global phases of ψ_1 and ψ_{-1} to obtain maximum localization. In our case, without losing generality, one can set the phases of $\psi_1(r,\theta,z)$ and $\psi_{-1}(r,\theta,z)$ to zero at the bisectrix $\theta = \pi/4$ and $z = 0$. And taking into account that $\psi_1 = \psi_{-1}^*$, it is sufficient to consider a single variational parameter η in their phases as $e^{\pm i\eta}\psi_{\pm 1}$ to analyze the localization of the Wannier function. The localized state w_k as a function of η thus acquires the form

$$w_k(r,\theta,z,\eta) = \tfrac{1}{2}\{\psi_0(r,\theta,z) + \psi_2(r,\theta,z)\cos k\pi + 2\mathrm{Re}[e^{i(\eta - k\pi/2)}\psi_1(r,\theta,z)]\}, \tag{6}$$

with the conditions on each $\psi_n(r,\theta,z)$ given above.

The maximum localization is achieved by minimizing the spatial dispersion of the WL wave functions in the xy plane $\sigma^2 = \langle x^2 + y^2\rangle - (\langle x\rangle^2 + \langle y\rangle^2)$ with respect to η. The degree of localization of the WL wave functions strongly affects the values of the model parameters. This is shown in Fig. 2 where we depict the calculated on-site interaction energy U as a function of η, together with the dispersion σ. Whereas the hopping parameters turn out to be rather independent of this phase, the parameter $U(\eta)$ has been shown to be strongly dependent. Such a variation would qualitatively alter the dynamics predicted by multimode models, thus demonstrating the importance of a properly localized wave function.

In Fig. 3, we show the three-dimensional WL function density w_0^2 at $z = 0$ with $\eta = 0$ and $\eta = \pi/4$, showing that in the first case it is clearly more localized.

In summary, to obtain an accurate MM dynamics, one should achieve the maximum localization of the WL functions,

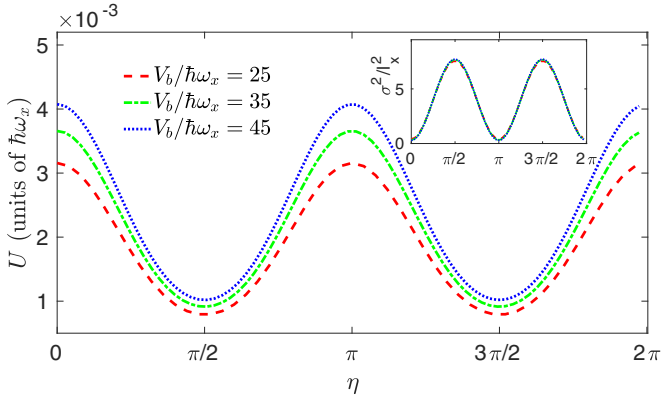

FIG. 2. Bare on-site interaction energy parameter U as a function of the phase η. The inset shows the dispersion σ of the WL functions in the xy plane as a function of η, with $l_x = l_y = \sqrt{\hbar/(m\omega_x)}$.

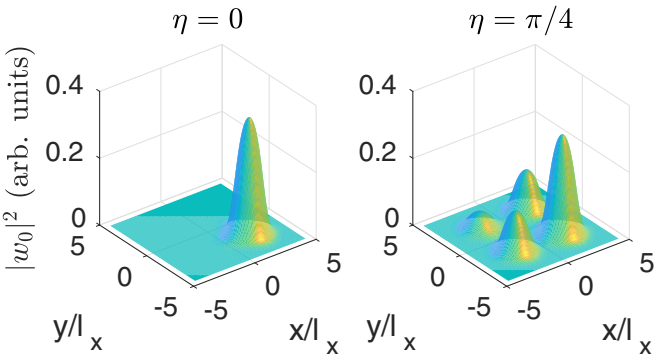

FIG. 3. WL wave-function densities $|w_0|^2$ (in arbitrary units) at the $z = 0$ plane for $\eta = 0$ (left panel) and $\eta = \pi/4$ (right panel).

which is found to be fulfilled when the phases of all stationary states are chosen equal at the bisectrix of a given site.

D. Inclusion of effective on-site interaction effects

In addition to the localization effects, to construct an accurate model we need to calculate the effective on-site interaction energy parameter $U_{\rm eff}$. For that matter, we follow the procedure described in Ref. [8] valid for a ring-shaped lattice with equal wells. We thus first numerically calculate the on-site interaction energy $U_k(\Delta N_k)$ in the k site as a function of $\Delta N_k = N_k - N/N_c$ as [8]

$$\frac{U_k(\Delta N_k)}{U} = \frac{\int d^3\mathbf{r}\rho_N(\mathbf{r})\rho_{N+\Delta N}(\mathbf{r})}{\int d^3\mathbf{r}\rho_N^2(\mathbf{r})}, \tag{7}$$

with the normalized-to-unity ground-state densities ρ_N and $\rho_{N+\Delta N}$ for four-well systems of N and $N + \Delta N$ total number of particles, respectively, where $\Delta N = N_c\Delta N_k$. The on-site interaction energy U_k exhibits a linear dependence on ΔN_k and it can be approximated by

$$\frac{U_k(\Delta N_k)}{U} \simeq 1 - \alpha\frac{N_c\Delta N_k}{N}. \tag{8}$$

Replacing $U_{k-1}(\Delta N_{k-1})$ and $U_k(\Delta N_k)$ given by the above equation in Eq. (4), the effective multimode (EMM) model equations of motion read

$$\begin{aligned}
\hbar\frac{dn_k}{dt} &= -2J[\sqrt{n_k n_{k+1}}\,\sin\varphi_{k+1} - \sqrt{n_k n_{k-1}}\,\sin\varphi_k] \\
&\quad - 2F[\sqrt{n_k n_{k+1}}(n_k + n_{k+1})\,\sin\varphi_{k+1} - \sqrt{n_k n_{k-1}}(n_k + n_{k-1})\,\sin\varphi_k], \qquad (9)\\
\hbar\frac{d\varphi_k}{dt} &= f_{3D}(n_{k-1} - n_k)NU - \alpha(n_{k-1} - n_k)NU[N_c(n_{k-1} + n_k) - 2] \\
&\quad - J\left[\left(\sqrt{\frac{n_k}{n_{k-1}}} - \sqrt{\frac{n_{k-1}}{n_k}}\right)\cos\varphi_k + \sqrt{\frac{n_{k-2}}{n_{k-1}}}\cos\varphi_{k-1} - \sqrt{\frac{n_{k+1}}{n_k}}\cos\varphi_{k+1}\right] \\
&\quad - F\left[\left(n_k\sqrt{\frac{n_k}{n_{k-1}}} - n_{k-1}\sqrt{\frac{n_{k-1}}{n_k}}\right)\cos\varphi_k + \left(3\sqrt{n_{k-2}n_{k-1}} + n_{k-2}\sqrt{\frac{n_{k-2}}{n_{k-1}}}\right)\cos\varphi_{k-1}\right. \\
&\quad \left. - \left(3\sqrt{n_{k+1}n_k} + n_{k+1}\sqrt{\frac{n_{k+1}}{n_k}}\right)\cos\varphi_{k+1}\right], \qquad (10)
\end{aligned}$$

where $f_{3D} = 1 - \alpha$, and hence we obtain $U_{\rm eff} = f_{3D}U$.

In Table I, we quote the values of α and f_{3D} for a few configurations and observe that for larger particle numbers and higher barrier heights, the parameter f_{3D} approaches from above the three-dimensional (3D) Thomas-Fermi limiting value of 7/10, derived for the double-well model [21]. Also, it is worthwhile noticing that the second term of the right-hand side of Eq. (10) is a second-order correction on the population imbalance, which in general does not give rise to noticeable changes in the dynamics.

TABLE I. Linear coefficient α of the on-site interaction energy U_k and factor f_{3D} for $N_c = 4$ and different number of particles and barrier heights.

N	$V_b/(\hbar\omega_x)$	α	f_{3D}
10^3	10	0.20	0.80
10^3	15	0.20	0.80
10^4	25	0.28	0.72
10^4	35	0.29	0.71

III. THE DYNAMICS

A. TM symmetric case

The orbits of the dynamical equations lie in a six-dimensional space, and thus it becomes challenging to classify them taking into account the possible different features. In particular, it is important to predict the regions of self-trapped and Josephson trajectories, where in the multiwell system we define a self-trapped site k as a site whose population difference with neighboring sites $N_k - N_{k\pm1}$ does not change sign during the whole time evolution [7]. A subset of such trajectories can be found by restricting the dynamics to a more symmetric case, which can be described with a TM Hamiltonian.

Therefore, we will first analyze the multimode model in a symmetric case where $n_k = n_{k+2}$ and $\varphi_k = \varphi_{k+2}$. In this case, the second term on the right-hand side of Eq. (10) vanishes, and the only difference between the MM and EMM equations of

motion is given by the use of the effective interaction parameter $U_{\rm eff}$ instead of the bare U.

Defining the imbalance $Z = 2(N_0 - N_1)/N$, the phase difference $\varphi = \varphi_1$, and $K = 2J + F$, the equations of motion given by Eqs. (9) and (10) reduce to

$$\hbar \frac{dZ}{dt} = -2K\sqrt{1-Z^2}\sin\varphi, \tag{11}$$

$$\hbar \frac{d\varphi}{dt} = \frac{U_{\rm eff}}{2} NZ + 2K \frac{Z}{\sqrt{1-Z^2}}\cos\varphi. \tag{12}$$

Then, changing for convenience the time units to $\hbar/2K$, one can obtain a TM-type Hamiltonian for the reduced space,

$$H(Z,\varphi) = \tfrac{1}{2}\Lambda Z^2 - \sqrt{1-Z^2}\cos\varphi, \tag{13}$$

where $\Lambda = U_{\rm eff} N/(4K)$.

We can thus obtain the critical imbalance between the Josephson and ST regimes,

$$Z_c = 2\frac{\sqrt{\Lambda - 1}}{\Lambda}, \tag{14}$$

and calculate the exact time periods $T^{\rm EMM}$ using Λ [10,22], together with the approximations obtained in the small-oscillation limit,

$$T^{\rm EMM}_{\rm so} = \frac{\pi\hbar}{K\sqrt{\Lambda + 1}}, \tag{15}$$

and in the ST regime [22],

$$T^{\rm EMM}_{\rm st} = \frac{Z_i \pi \hbar}{2K}\left(1 - \sqrt{1 - \frac{4}{\Lambda Z_i^2}}\right), \tag{16}$$

where Z_i is the initial imbalance.

For the system with $N = 10^4$ particles and a barrier height $V_b = 25\,\hbar\omega_x$, we have obtained $J = -6.60 \times 10^{-4}\hbar\omega_x$, $F = 2.08 \times 10^{-3}\hbar\omega_x$, $U = 3.16 \times 10^{-3}\hbar\omega_x$, and $U_{\rm eff} = 2.27 \times 10^{-3}\hbar\omega_x$, which yields a critical imbalance $NZ_c = 232$ within the EMM model. On the other hand, using the bare value of U, we would have obtained a smaller threshold $NZ_c = 196$. For the same system, the small-oscillation period yields $T^{\rm EMM}_{\rm so} = 47.84\omega_x^{-1}$, which may be compared to that obtained by means of GP simulations, $T^{\rm GP}_{\rm so} \simeq 47.7\omega_x^{-1}$. In Fig. 4, we show the time evolution for the initial $NZ_i = 120 < NZ_c$ in the Josephson regime, within the GP, MM, and EMM frameworks. It is worthwhile noticing that although the period for this value of Z_i departs from the small-oscillation limit, the GP and exact EMM are in good agreement.

In Fig. 5, we show the evolution of the populations in each site for the initial condition $N_0 = 2640$ and $N_1 = 2360$. In this case $NZ_i = 560 > NZ_c$ and then the system is in the ST regime. We may further calculate the period from Eq. (16), using in this case $Z_i = 0.056$ yielding $T^{\rm EMM}_{\rm st} = 10.391\,\omega_x^{-1}$, which turns out to be in a good agreement with the GP simulation and EMM model results, $T^{\rm EMM} = 10.396\,\omega_x^{-1}$.

B. Near the TM symmetric case

In the TM symmetric situation of the previous section, the system is governed by the TM Hamiltonian, given by Eq. (13), and thus the orbits are periodic. However, for arbitrary nonsymmetric initial conditions, the dynamics become nonperiodic in general. To investigate this scenario, we perform a linear analysis of the six-dimensional dynamical system around the TM symmetric case. With this aim, we first rewrite the time-evolution equations in terms of the mean populations and phases of non-neighboring sites $\bar{n}_{ij} = (n_i + n_j)/2$, $\bar{\varphi}_{ij} = (\varphi_i + \varphi_j)/2$, and corresponding differences $\boldsymbol{\delta}$ (see Appendix B). Then, linearizing the resulting dynamical equations in the differences, we obtain two sets of equations. On the one hand, we recover the TM equations for $Z = 2(\bar{n}_{02} - \bar{n}_{13})$ and $\varphi = \bar{\varphi}_{13}$. And, on the other hand, we obtain a nonautonomous linear system for the differences, which can be cast as

$$\frac{d\boldsymbol{\delta}}{dt} = \mathbb{A}[Z(t),\varphi(t)]\boldsymbol{\delta}, \tag{17}$$

where the vector $\boldsymbol{\delta}$ is defined as the following differences:

$$\boldsymbol{\delta} = \tfrac{1}{2}(n_0 - n_2, \varphi_0 + \varphi_3 - \varphi_1 - \varphi_2, \times n_1 - n_3, \varphi_0 + \varphi_1 - \varphi_2 - \varphi_3). \tag{18}$$

The periodicity of $Z(t)$ and $\varphi(t)$ gives rise to a Floquet problem for $\boldsymbol{\delta}$ [23]. Therefore, we shall pursue the study of the characteristic multipliers ρ_j as functions of the initial imbalance $Z(0) = Z_i$ and $\varphi(0) = 0$. The multipliers are the eigenvalues of the monodromy matrix $\mathbb{M}$ associated to Eq. (17) [23] and they contain information on the evolution of $\boldsymbol{\delta}$ after a period T, since $\boldsymbol{\delta}(T) = \mathbb{M} \cdot \boldsymbol{\delta}(0)$. In particular, each multiplier

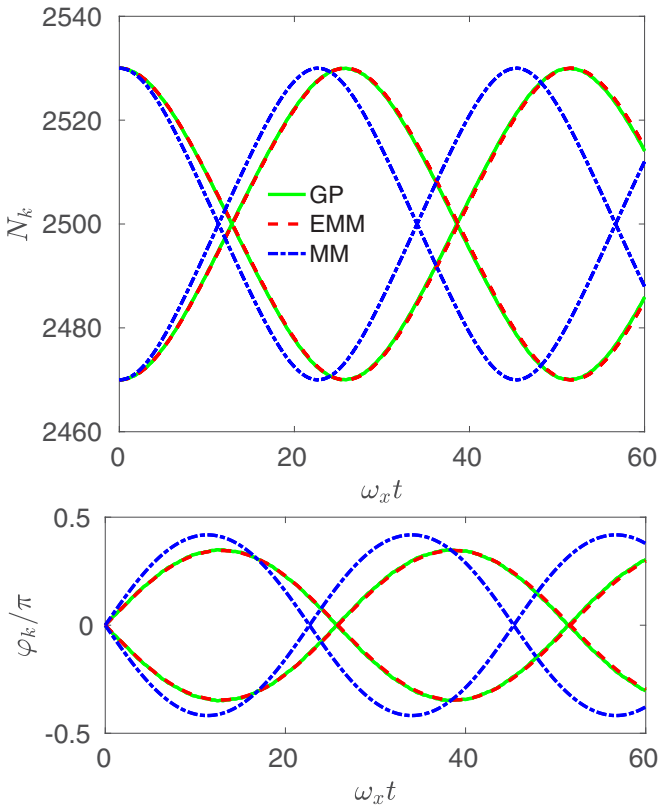

FIG. 4. Condensate dynamics arising from the GP equation, and from the EMM and the MM models for an initial condition $N_0 = 2530$ and $N_1 = 2470$ corresponding to the Josephson regime. Top panel: Populations in each well N_k. Bottom panel: Phase differences φ_k.

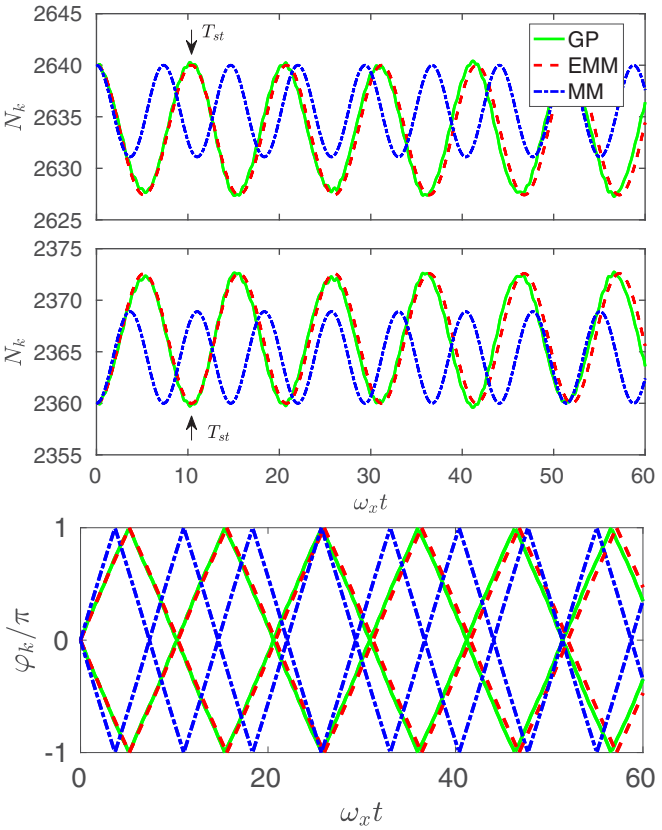

FIG. 5. Condensate dynamics for the initial values $N_0 = 2640$, and $N_1 = 2360$ in the ST regime. We depict the GP simulation result, together with those arising from the EMM and MM models. Top panel: Populations in each well N_k. Bottom panel: Phase differences φ_k.

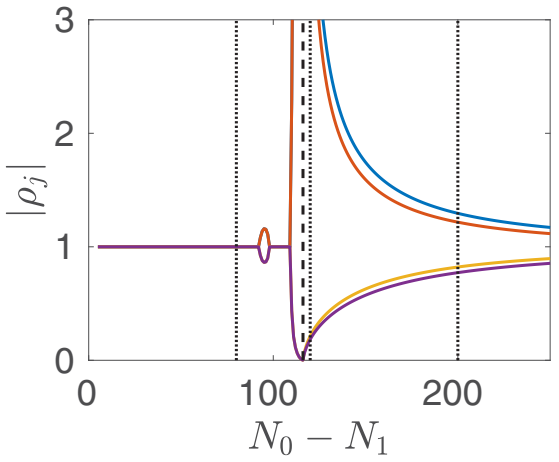

FIG. 6. Characteristic Floquet multipliers for the orbits of the effective TM model as functions of the initial values of $N_0 - N_1$. The dashed line marks the critical condition $N_0 - N_1 = 116$ for the transition between Josephson and ST regimes, and the dotted ones indicate the initial values of $N_0 - N_1$ for the evolutions shown in Fig. 7.

ρ_j gives the ratio of change of a linearly independent solution $\boldsymbol{\delta}_j$, i.e., $\boldsymbol{\delta}_j(T) = \rho_j \boldsymbol{\delta}_j(0)$. Each Floquet multiplier thus falls into one of the following categories that characterize the dynamics of the solutions:

(1) If $|\rho_j| < 1$, there is a solution $\boldsymbol{\delta}_j$ that is asymptotically stable.

(2) If $|\rho_j| = 1$, we have a pseudoperiodic solution. If $\rho_j = \pm 1$, then the solution is periodic.

(3) If $|\rho_j| > 1$, there is a linearly unstable solution $\boldsymbol{\delta}_j(t)$.

The entire solution is asymptotically stable if all the characteristic multipliers satisfy $|\rho_j| \leqslant 1$. In Fig. 6, we show the absolute value of the four Floquet multipliers for the periodic orbits of Sec. III A. Given that $\mathrm{Tr}(\mathbb{A}) = 0$ and the fact that the matrix $\mathbb{A}$ is decoupled into blocks of 2×2 matrices, the product of the eigenvalues verifies $\rho_1\rho_2 = 1$ and $\rho_3\rho_4 = 1$. As it may be seen, far from the critical imbalance in the Josephson regime, the dynamics is pseudoperiodic, whereas for the ST regime, the linear dynamics is unstable. We also observe a small region, $0.0185 \lesssim Z \lesssim 0.0195$, where two multipliers exceed the value 1, indicating that the effect of the instability extends towards the Josephson regime. From this analysis, one may conclude that near symmetric initial conditions in the Josephson regime, the dynamics of the exact model is almost always close to that of the effective TM model, while for initial conditions around the ST regime, the Floquet analysis predicts linear instability, and thus the nonlinearized dynamics are expected to differ considerably from the effective TM results. However, for a particular evolution, one should also inspect the involved values of the monodromy matrix elements to understand in more detail the initial deviation from the TM orbits. This behavior is illustrated in Fig. 7, where we plot the numerical solutions of the EMM dynamics for several initial conditions with a small $(n_0 - n_2)/(2Z) = 0.1$, $N_1 = N_3$, and zero phases. Furthermore, it can be easily shown that the choice of zero phases and $N_1 = N_3$ as initial conditions warrants that the dynamics can be described in terms of four variables only, namely, Z, φ and the differences $N_0 - N_2$ and $\varphi_0 - \varphi_2$, instead of the full six dimensions, as can be expected from the symmetry of such configuration.

As a consequence of the linear instability, it is not possible to reliably predict the full dynamics close to Z_c only from the TM Hamiltonian and a numerical solution of the EMM model must be performed for each initial condition. This is clearly shown in the middle panel of Fig. 7 with $Z_i \gtrsim Z_c$, where the shape of the oscillations of N_k is depicted. Nonetheless, already for slightly larger values of Z_i where all the $|\rho_j|$ are closer to one, we observe that there is a characteristic time close to the time-period prediction of the TM model, $T \simeq T^{\mathrm{EMM}}(Z_i)$. In addition to T, as seen clearly in the bottom panel of Fig. 7, there is a beat-type oscillation with a much longer characteristic time, $T_M \approx 16T$. This beating can be understood as the composition of two ST modes for each pair of neighbors with nearby time periods T_1 and T_2 given by Eq. (16), leading to the modulating period $T_M = 2T_1T_2/(T_1 - T_2)$.

The change in the population imbalance after a single period T can be read off directly from the monodromy matrix. In particular, for the initial conditions of Fig. 7, the element of the matrix $\mathbb{M}_{11}$ corresponds to the ratio $\delta_1(T)/\delta_1(0)$, shown in Fig. 8. In the Josephson regime for $Z < 0.0215$, $\delta_1(t)$ changes sign and reduces its magnitude after a period, as can be seen in the top panel of Fig. 7, whereas for $Z_i = 0.04$ in the ST regime, we observe that $\delta_1(t)$ does not change after a period T (bottom panel of Fig. 7).

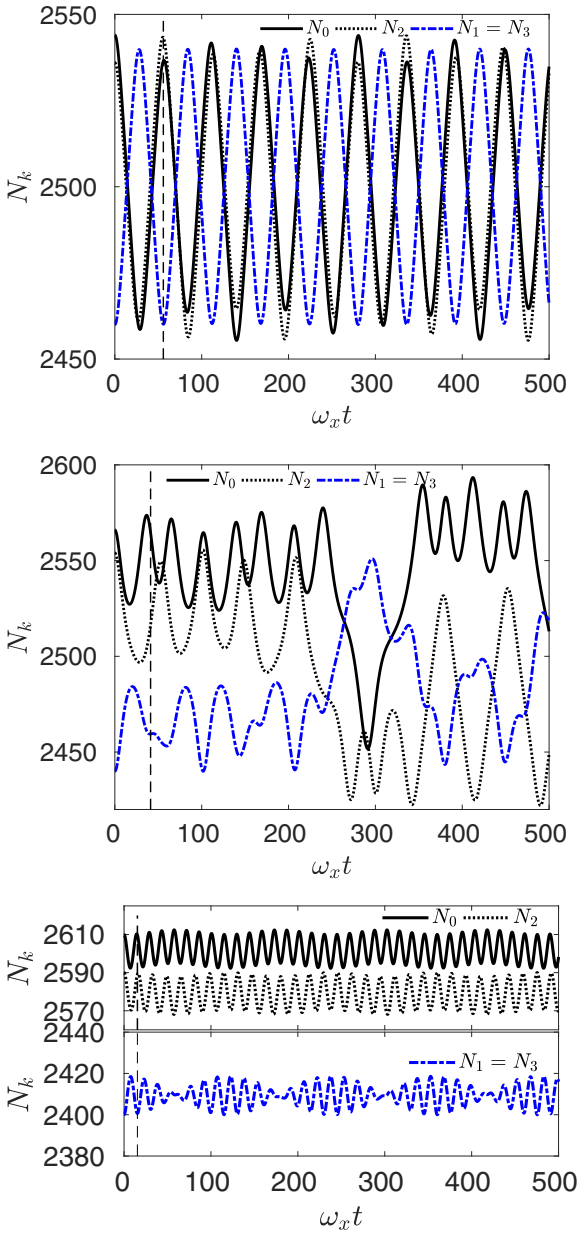

FIG. 7. Time evolution of the populations N_k for initial conditions close to the TM symmetric case for $Z_i = 0.016$ (top), 0.024 (middle), and 0.04 (bottom), and $(n_0 - n_2)/(2Z_i) = 0.1$. The vertical dashed lines mark the orbit periods for the effective TM model at each value of Z_i.

C. Regimes in the $N_1 = N_3$ symmetric case

In addition to the investigation of the characteristic times, it is interesting to wonder whether the system could remain in a Josephson or in a ST regime in the surrounding region of a given TM symmetric configuration. Therefore, we have studied the EMM equations of motion for $n_i(t)$ and $\varphi_i(t)$ for several initial conditions in a specific plane of the full phase space containing the symmetric configuration. In particular, we numerically integrated Eqs. (9) and (10) from $t = 0$ to $t = 500\omega_x^{-1}$ with fixed initial phase differences $\varphi_i = 0$ and $N_1 = N_3$, while varying $N_0 - N_1$ and $N_2 - N_3$. We classify

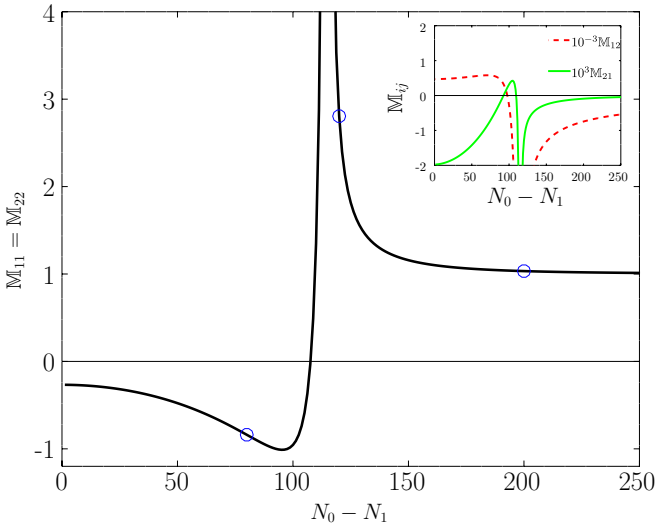

FIG. 8. Monodromy matrix elements $\mathbb{M}_{ij}$ as functions of the initial imbalance $N_0 - N_1$. The empty circles mark the values corresponding to Fig. 7.

the dynamics for each initial condition in one of the following three regimes: Josephson (J), mixed (M), and self-trapping (ST), depending on whether all (J), some (M), or none (ST) of the populations of neighboring sites cross each other during the time evolution.

Assuming the double-well condition for a ST regime [cf. Eq. (14)] for each pair of neighbors forming a junction, one can obtain a first estimate of the phase-space domains of the J,

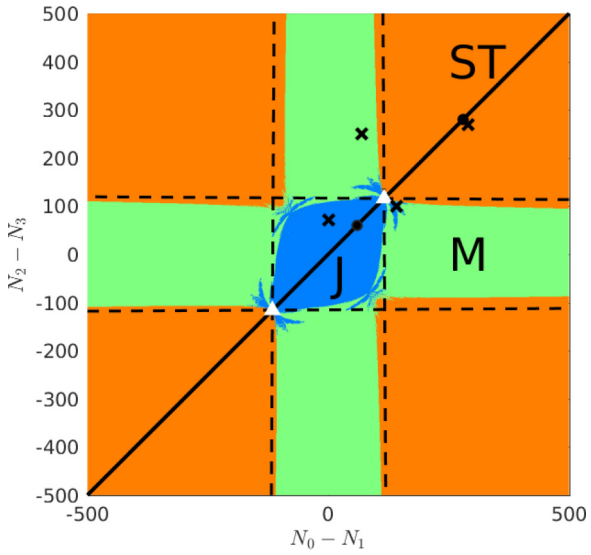

FIG. 9. Phase-space diagram of the four-mode model with $\varphi_i = 0$ and $N_1 = N_3$. The solid line marks the symmetric case with $N_0 = N_2$ and $N_1 = N_3$. The dashed lines indicate the local conditions $A_{ij} = B_{ij}$. The triangles correspond to the critical condition $N_0 - N_1 = N_2 - N_3 = \pm 116$ extracted from Eq. (14), the circles indicate the symmetric initial conditions of Figs. 4 and 5, and the crosses indicate the nonsymmetric ones in Figs. 10–13.

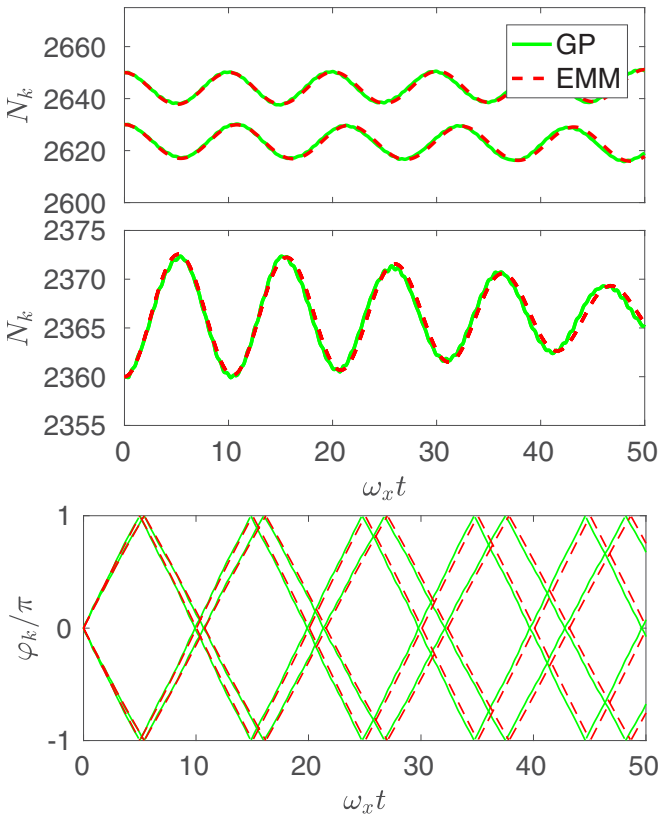

FIG. 10. Dynamics arising from the GP simulation and the EMM model, for initial values $N_0 = 2650, N_1 = 2360, N_2 = 2630$, and $N_3 = 2360$, with $V_b/(\hbar\omega_x) = 25$. Top panel: Populations N_k. Bottom panel: Phase differences φ_k.

M, and ST regimes. Thus, defining the parameters

$$A_{ij} = (N_i - N_j)^2 \frac{U_{\text{eff}}}{2K} \quad \text{and} \quad B_{ij} = 4(N_i + N_j) - \frac{8K}{U_{\text{eff}}}, \tag{19}$$

the populations of neighboring sites i and j should cross each other when $A_{ij} < B_{ij}$. Therefore, if this condition is fulfilled for the four junctions, we expect a J regime; if no junction satisfies it, we expect a ST regime; and a mixed regime otherwise. Similar local two-mode model conditions have been considered in the study of self-trapping in extended one-dimensional optical lattices [18,19].

In Fig. 9, we show a phase-space diagram resulting from the numerical integration of the EMM dynamics together with the local predictions implied by Eqs. (19). We observe that in the neighborhood of a symmetric configuration not immediate to the critical point, the character of the regime does not change, i.e., a ST regime remains as ST, and so does a J regime. Only in the close vicinity of the critical point in the symmetric configuration do we numerically observe that the dynamics possesses qualitative details not contained in the local analysis of Eq. (19). This result was expected from the Floquet analysis of the previous section, where the absolute value of some multipliers greatly exceeded 1 around Z_c. The detailed study of such phase-space regions deserves a separate and careful numerical analysis, which lies beyond the scope of the present work.

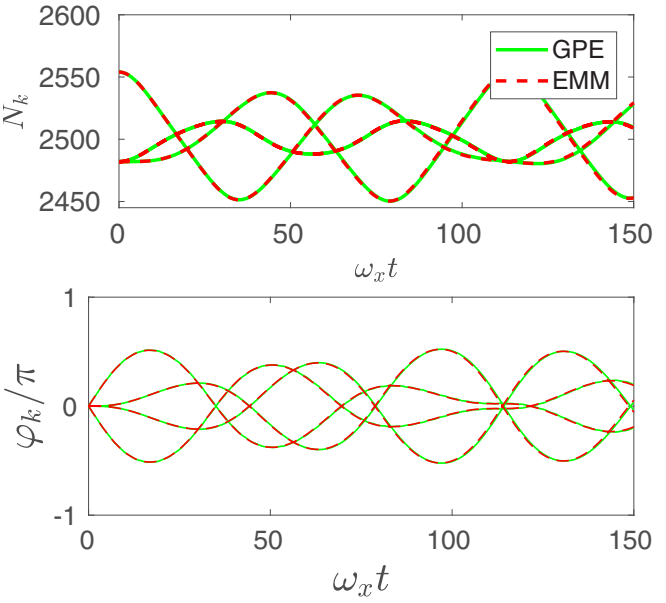

FIG. 11. Same as Fig. 10 for $N_0 = 2482$, $N_1 = 2482$, $N_2 = 2554$, and $N_3 = 2482$.

To verify our findings within the framework of the full GP equations, we have numerically solved several nonsymmetric initial conditions. First, we slightly move from the symmetric point in the ST regime in Fig. 5 and choose $N_0 = 2650$, $N_1 = 2360$, $N_2 = 2630$, and $N_3 = 2360$. We show in Fig. 10 the

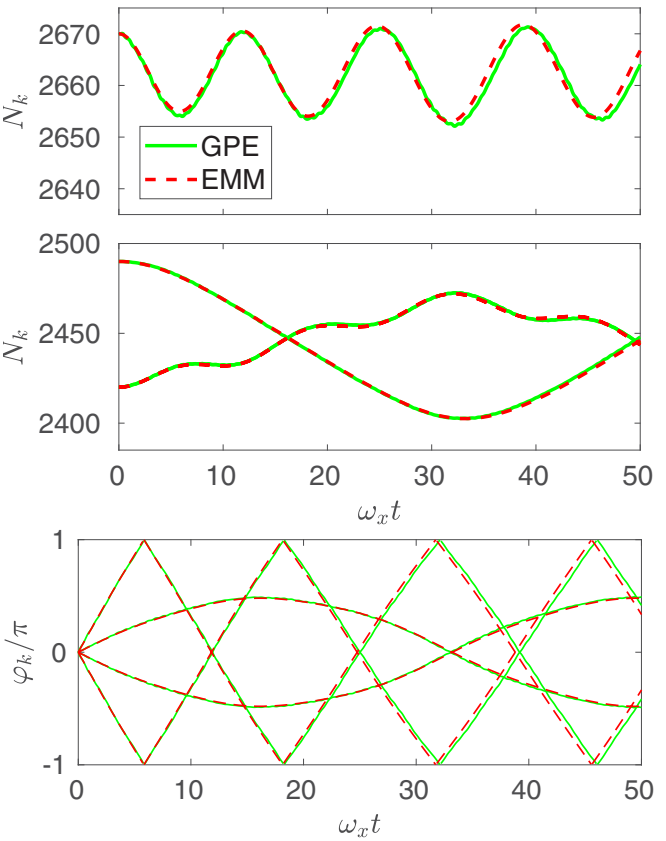

FIG. 12. Same as Fig. 10 for $N_0 = 2490, N_1 = 2420, N_2 = 2670$, and $N_3 = 2420$.

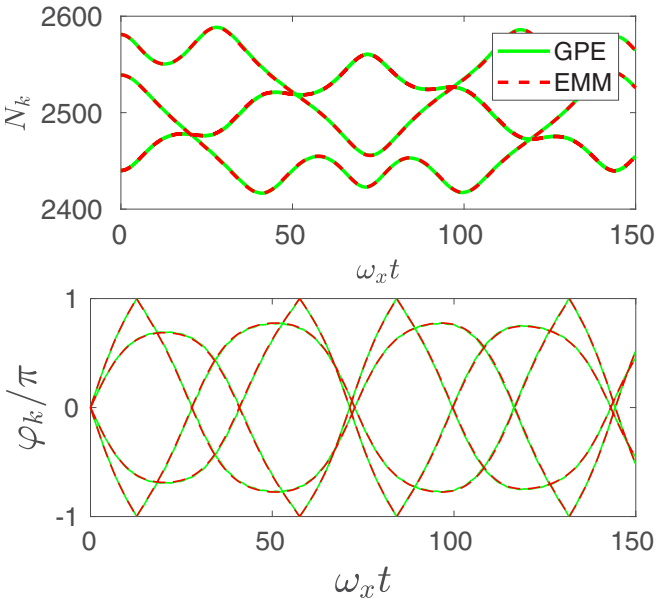

FIG. 13. Same as Fig. 10 for $N_0 = 2581$, $N_1 = 2440$, $N_2 = 2539$, and $N_3 = 2440$.

corresponding time evolution. We note that the characteristic times in the surrounding region of the symmetric case smoothly depart from the orbit periods of the two-mode models. In particular, it can be seen that in Fig. 10, the oscillation times keep around $10\omega_x^{-1}$, very close to that of Fig. 5, although this simulation does not correspond to a closed orbit. Similarly, in Fig. 11, we compare the time evolutions in the Josephson regime within the GP and EMM approaches, finding an excellent agreement.

We present in Fig. 12 another example of a nonsymmetric initial condition within the GP equations, where we expect that this time it will be in a mixed regime. We take the initial populations $N_0 = 2490, N_1 = 2420, N_2 = 2670$, and $N_3 = 2420$. Note that in Fig. 12 some of the initial population differences lie below the critical threshold obtained for the symmetric case, and these conditions turn out to be useful for predicting that this state would be in a mixed regime also in the GP framework.

Finally, in Fig. 13, we show the GP evolution for a particular initial condition which, according to the simplified local model, should have been in the mixed regime but, as predicted within the EMM model, is in a Josephson regime.

To conclude, from the previous analysis it can be seen that the study of symmetric configurations is a convenient starting point for exploring the full six-dimensional system (n_i, φ_i) arising from the four-mode model. We have shown that the adoption of TM tools allows us to predict different regimes and characteristic times for the dynamics of four-site condensates. These results may be easily extended to condensates with a larger even number of sites.

IV. SUMMARY AND CONCLUDING REMARKS

We have studied the dynamics of three-dimensional four-well Bose-Einstein condensates using a multimode model with an effective interaction parameter, and compared it to the Gross-Pitaevskii solutions. In order to predict orbits in four-well systems and to establish the characteristic time scales of the dynamics, we have first studied a highly symmetric configuration that admits a two-mode Hamiltonian description. This allowed us to apply previous two-mode results to this reduced-space case. Moreover, the location of the critical point marking the transition from Josephson to self-trapping regimes in the symmetric case has been useful for defining, in the extended phase space, zones with different dynamical regimes. For general initial conditions close to the two-mode symmetric ones, we performed a Floquet analysis that revealed that the linearized dynamics is unstable around the critical imbalance points. The linear instability in the Floquet problem explains the coexistence of different regimes in the neighborhood of the critical imbalance in the extended phase space.

We have characterized the possible dynamical regimes according to the population behavior between neighboring sites. Hence, we have performed a partition of an extended region of the phase space into self-trapped, Josephson, and mixed regimes. We have confirmed these findings by an extensive numerical study of nonsymmetric initial conditions within the multimode model, together with a set of time evolutions within the three-dimensional Gross-Pitaevskii framework.

We must emphasize that the accuracy of the predictions of the multimode model depends on the proper determination of its parameters. On the one hand, we have obtained very good agreements due to the use of the effective on-site interaction energy parameter $U_{\rm eff}$. Such a parameter amounts to a reduction of about a factor 0.72 with respect to the bare U of Eq. (A2). On the other hand, we have also shown that U strongly depends on the localization of the underlying Wannier-like functions. Such a localization has to be maximized in order to obtain an accurate model. This can be achieved by minimizing its spatial dispersion with respect to a parameter that defines the global phases of the stationary states with $n = \pm 1$ winding numbers. This procedure should also be applied to systems with a larger number of sites, where more stationary states with nonzero velocity circulations exist, and therefore another variational parameter has to be added for each new absolute value of the winding number.

To conclude, we would like to remark that the present study of four-well systems could pave the way for an eventual generalization to condensates with a higher number of sites.

ACKNOWLEDGMENTS

This work was supported by CONICET and Universidad de Buenos Aires through Grants No. PIP 11220150100442CO and No. UBACyT 20020150100157BA, respectively.

APPENDIX A: MULTIMODE PARAMETERS

The parameters of the MM mode are defined as

$$J = -\int d^3\mathbf{r}\; w_0(\mathbf{r})\left[-\frac{\hbar^2}{2m}\nabla^2 + V_{\rm trap}(\mathbf{r})\right] w_1(\mathbf{r}), \tag{A1}$$

$$U = g\int d^3\mathbf{r}\; w_0(\mathbf{r})^4, \tag{A2}$$

$$F = -gN\int d^3\mathbf{r}\; w_0^3(\mathbf{r}) w_1(\mathbf{r}). \tag{A3}$$

The parameter F were first defined in Ref. [11] and later analyzed in Ref. [12].

Together with the calculation of these parameters through the preceding definitions, we have also applied the alternative method outlined in Ref. [24], finding an agreement between both procedures with a precision higher than 99%. For the MM model applied to the four-well system, the hopping parameter can be written as

$$\Delta E = E_2 - E_0 = 4J + 2F = 2K, \tag{A4}$$

where E_2 is the energy of the stationary state with winding number $n = 2$ and E_0 is the energy of the ground state. It is interesting to note that one can also assure that we have used high enough barriers, provided the parameters calculated through the definitions (A1)–(A3) are in agreement with the corresponding results arising from the above alternative method. For example, in our numerical calculation $V_b = 25\,\hbar\omega_x$ and we get $E_2 - E_0 = 1.5251 \times 10^{-3}\,\hbar\omega_x$, whereas by definition we obtained $2K = 1.525 \times 10^{-3}\hbar\omega_x$. On the other hand, if using $V_b = 15\hbar\omega_x$, we get $E_2 - E_0 = 8.78 \times 10^{-2}\hbar\omega_x$, being by definition $2K = 8.85 \times 10^{-2}\hbar\omega_x$, which clearly reflects a less accurate model.

APPENDIX B: LINEARIZED DYNAMICS AROUND PERIODIC ORBITS

Starting from the dynamical equations (9) and (10), we make a change of variables to the mean values,

$$\begin{aligned} \bar{n}_{02} &= (n_0 + n_2)/2, \quad \bar{n}_{13} = (n_1 + n_3)/2, \\ \bar{\varphi}_{02} &= (\varphi_0 + \varphi_2)/2, \quad \bar{\varphi}_{13} = (\varphi_1 + \varphi_3)/2, \end{aligned} \tag{B1}$$

and the differences,

$$\begin{aligned} \delta_1 &= (n_0 - n_2)/2, \quad \delta_3 = (n_1 - n_3)/2, \\ \delta_2 &= (\varphi_0 + \varphi_3 - \varphi_2 - \varphi_1)/2, \quad \delta_4 = (\varphi_0 + \varphi_1 - \varphi_2 - \varphi_3)/2. \end{aligned} \tag{B2}$$

Linearizing the resulting equations on the differences δ_i and taking into account that $\bar{n}_{02} + \bar{n}_{13} = N/2$ and $\bar{\varphi}_{02} = -\bar{\varphi}_{13}$, we obtain two sets of equations. On the one hand, the mean values are decoupled from the differences $\boldsymbol{\delta}$ and thus there are only two independent equations, namely,

$$\hbar\dot{\bar{n}}_{02} = \frac{K}{2}\sin\bar{\varphi}_{02}\sqrt{1 - Z^2}, \tag{B3}$$

$$\hbar\dot{\bar{\varphi}}_{02} = -\frac{U_{\rm eff}N}{2}Z - 2KZ\frac{\cos\bar{\varphi}_{02}}{\sqrt{1 - Z^2}}. \tag{B4}$$

On the other hand, for δ_i, we obtain

$$\begin{aligned} \hbar\,\dot{\delta}_1 &= -\sqrt{1 - Z^2}\left(F + \frac{K}{1 + Z}\right)\sin\varphi\,\delta_1 + \frac{1}{4}\sqrt{1 - Z^2}K\cos\varphi\,\delta_2, \\ \hbar\,\dot{\delta}_2 &= \left[-2(U_{\rm eff} - 2\alpha ZU)N + 4\frac{1 - Z}{\sqrt{1 - Z^2}}\left(2F - \frac{K}{1 + Z}\right)\cos\varphi\right]\delta_1 + \sqrt{1 - Z^2}\left(F + \frac{K}{1 + Z}\right)\sin\varphi\,\delta_2, \end{aligned} \tag{B5}$$

$$\begin{aligned} \hbar\,\dot{\delta}_3 &= \sqrt{1 - Z^2}\left(F + \frac{K}{1 - Z}\right)\sin\varphi\,\delta_3 + \frac{1}{4}\sqrt{1 - Z^2}K\cos\varphi\,\delta_4, \\ \hbar\,\dot{\delta}_4 &= \left[-2(U_{\rm eff} + 2\alpha ZU)N + 4\frac{1 + Z}{\sqrt{1 - Z^2}}\left(2F - \frac{K}{1 - Z}\right)\cos\varphi\right]\delta_3 - \sqrt{1 - Z^2}\left(F + \frac{K}{1 - Z}\right)\sin\varphi\,\delta_4, \end{aligned} \tag{B6}$$

where $Z = Z(t) = 2(\bar{n}_{02} - \bar{n}_{13})$ and $\varphi(t) = -\bar{\varphi}_{02} = -\bar{\varphi}_{02}(t)$ are the solutions of Eq. (B4) for a periodic orbit of the TM model. The equations for $\boldsymbol{\delta}$ can thus be cast as the matrix equation

$$\frac{d\boldsymbol{\delta}}{dt} = \mathbb{A}[Z(t),\varphi(t)]\boldsymbol{\delta}, \tag{B7}$$

where the matrix $\mathbb{A}$ is formed by two uncoupled blocks of 2×2 [cf. Eqs. (B5) and (B6)] for the (δ_1,δ_2) and (δ_3,δ_4) differences, respectively. Given the periodicity of $Z(t)$ and $\varphi(t)$, the dynamical system defines a Floquet problem [23]. To analyze the stability of the system, we first construct the associated fundamental monodromy matrix. This can be constructed from the solution of Eq. (B7) evaluated at $t = T$, obtained from the solutions for the set of four initial conditions $\boldsymbol{\delta}_i(0) = \hat{e}_i$, with $\hat{e}_i$ the canonical vectors. The four solutions $\boldsymbol{\delta}_i(t)$ are then used as columns to form the monodromy matrix $\mathbb{M}$,

$$\mathbb{M} = [\boldsymbol{\delta}_1(T)|\boldsymbol{\delta}_2(T)|\boldsymbol{\delta}_3(T)|\boldsymbol{\delta}_4(T)]. \tag{B8}$$

Finally, the diagonalization of $\mathbb{M}$ provides the four Floquet characteristic multipliers.

[1] L. Amico, A. Osterloh, and F. Cataliotti, Phys. Rev. Lett. **95**, 063201 (2005).

[2] K. Henderson, C. Ryu, C. MacCormick, and M. G. Boshier, New J. Phys. **11**, 043030 (2009).

[3] F. Jendrzejewski, S. Eckel, T. G. Tiecke, G. Juzeliunas, G. K. Campbell, L. Jiang, and A. V. Gorshkov, Phys. Rev. A **94**, 063422 (2016).

[4] J. Dziarmaga, M. Tylutki, and W. H. Zurek, Phys. Rev. B **84**, 094528 (2011); **86**, 144521 (2012).

[5] L. Amico, D. Aghamalyan, F. Auksztol, H. Crepaz, R. Dumke, and L. C. Kwek, Sci. Rep. **4**, 4298 (2014).
[6] T. F. Viscondi and K. Furuya, J. Phys. A **44**, 175301 (2011).
[7] S. De Liberato and C. J. Foot, Phys. Rev. A **73**, 035602 (2006).
[8] D. M. Jezek and H. M. Cataldo, Phys. Rev. A **88**, 013636 (2013).
[9] A. Smerzi, S. Fantoni, S. Giovanazzi, and S. R. Shenoy, Phys. Rev. Lett. **79**, 4950 (1997).
[10] S. Raghavan, A. Smerzi, S. Fantoni, and S. R. Shenoy, Phys. Rev. A **59**, 620 (1999).
[11] D. Ananikian and T. Bergeman, Phys. Rev. A **73**, 013604 (2006).
[12] X. Y. Jia, W. D. Li, and J. Q. Liang, Phys. Rev. A **78**, 023613 (2008).
[13] M. Albiez, R. Gati, J. Fölling, S. Hunsmann, M. Cristiani, and M. K. Oberthaler, Phys. Rev. Lett. **95**, 010402 (2005).
[14] M. Melé-Messeguer, B. Juliá-Díaz, M. Guilleumas, A. Polls, and A. Sanpera, New J. Phys. **13**, 033012 (2011).
[15] M. Abad, M. Guilleumas, R. Mayol, M. Pi, and D. M. Jezek, Europhys. Lett. **94**, 10004 (2011).
[16] T. Mayteevarunyoo, B. A. Malomed, and G. Dong, Phys. Rev. A **78**, 053601 (2008); B. Xiong, J. Gong, H. Pu, W. Bao, and B. Li, *ibid.* **79**, 013626 (2009); Q. Zhou, J. V. Porto, and S. Das Sarma, *ibid.* **84**, 031607(R) (2011); B. Cui, L. C. Wang, and X. X. Yi, *ibid.* **82**, 062105 (2010); M. Abad, M. Guilleumas, R. Mayol, M. Pi, and D. M. Jezek, *ibid.* **84**, 035601 (2011).
[17] C. E. Creffield, Phys. Rev. A **75**, 031607(R) (2007); J.-K. Xue, A.-X. Zhang, and J. Liu, *ibid.* **77**, 013602 (2008); T. J. Alexander, E. A. Ostrovskaya, and Y. S. Kivshar, Phys. Rev. Lett. **96**, 040401 (2006); B. Liu, L.-B. Fu, S.-P. Yang, and J. Liu, Phys. Rev. A **75**, 033601 (2007).
[18] Th. Anker, M. Albiez, R. Gati, S. Hunsmann, B. Eiermann, A. Trombettoni, and M. K. Oberthaler, Phys. Rev. Lett. **94**, 020403 (2005).
[19] B. Wang, P. Fu, J. Liu, and B. Wu, Phys. Rev. A **74**, 063610 (2006).
[20] A. R. Kolovsky, Phys. Rev. A **82**, 011601(R) (2010); S. K. Adhikari, J. Phys. B **44**, 075301 (2011).
[21] D. M. Jezek, P. Capuzzi, and H. M. Cataldo, Phys. Rev. A **87**, 053625 (2013).
[22] M. Nigro, P. Capuzzi, H. M. Cataldo, and D. M. Jezek, Eur. Phys. J. D **71**, 297 (2017).
[23] C. Chicone, *Ordinary Differential Equations with Applications*, 2nd ed. (Springer, New York, 2006).
[24] H. M. Cataldo and D. M. Jezek, Phys. Rev. A **84**, 013602 (2011).
[25] N. Marzari, A. A. Mostofi, J. R. Yates, I. Souza, and D. Vanderbilt, Rev. Mod. Phys. **84**, 1419 (2012).
[26] E. P. Gross, Nuovo Cimento **20**, 454 (1961); L. P. Pitaevskii, Zh. Eksp. Teor. Fiz. **40**, 646 (1961) [Sov. Phys. JETP **13**, 451 (1961)].
[27] D. M. Jezek and H. M. Cataldo, Phys. Rev. A **83**, 013629 (2011).